ROBUST RECOVERY FOR APERTURE SYNTHESIS IMAGING

Liying Wei[*], *Stefan J. Wijnholds*[†], *and Paul Hurley*[‡]

[*]IBM Research - Netherlands, Amsterdam, The Netherlands
[†] Netherlands Institute for Radio Astronomy (ASTRON), Dwingeloo, The Netherlands
[‡]IBM Zurich Research Laboratory, Ruschlikon, Switzerland

ABSTRACT

We propose a sparse reconstruction method based on compressed sensing theory for aperture synthesis imaging. Our algorithm directly works on observational data without gridding. We achieve fast convergence by introducing an adaptive tolerance parameter based on the noise level and a thresholding value based on the cumulative sum of the power of the estimated source components. We demonstrate the accuracy in estimating the source positions and intensities in extremely low signal-to-noise (SNR) scenarios in Monte Carlo simulation. We could recover both point sources and extended sources with our algorithm using a Dirac basis from real data.

Index Terms— Interferometry, imaging, antenna array

1. INTRODUCTION

In radio astronomy, high-resolution, high-sensitivity and robust imaging is needed to recover the spatial intensity distribution of the celestial sources from a huge amount of incomplete and noisy covariance data. These data are obtained from large radio interferometers such as the Low Frequency Array (LOFAR) [1] and the Square Kilometre Array (SKA) [2]. Current standard imaging algorithms such as Högbom CLEAN [3], which starts from the dirty image and successively subtracts a user-defined fraction of the point spread function (PSF) around the brightest spots of the image, work well for point sources but often have difficulty with extended sources. Multiscale CLEAN [4] is designed to reconstruct extended objects. However, both of them are limited by the convergence speed.

Compressed sensing (CS) techniques, which can reconstruct a signal using far fewer measurements than required by the Nyquist-Shannon theory, have been proposed in interferometry for many years, but few of these algorithms are validated on observational data. Wiaux et al. [5] were the first to use the basis pursuit (BP) algorithm to recover the images of different radio sources from simulated measurements. Wenger et al. [6] proposed the SparseRI algorithm based on the iterative shrinkage/thresholding technique and evaluated it for the Very Large Array (VLA) telescope. As shown in simulations, SparseRI can reproduce the main features of the test sources, but it requires a resampling/gridding procedure to use the fast Fourier transform. Li et al. [7] proposed a CS-based deconvolution method by using the isotropic undecimated wavelet transform (IUWT) to reconstruct both point sources and extended sources. Carrillo et al. [8] proposed an analysis-based scalable algorithm, named sparsity averaging reweighted analysis (SARA), based on the simultaneous direction method of multipliers (SDMM) and evaluated it with simulated incomplete visibilities of a test image, for which the results demonstrated its superiority to the state-of-the-art imaging method. Garsden [9] implemented another synthesis-based sparse reconstruction method for the standard LOFAR imaging tool and verified its performance with both simulated and real LOFAR data. Onose et al. [10] proposed two new algorithms separately based on the alternating direction method of multipliers (ADMM) and primal-dual (PD) to solve the sparsity averaging optimisation problem proposed in [8] to achieve scalable processing for large datasets.

In this paper, we apply the Douglas-Rachford splitting algorithm [11] to solve the image reconstruction problem. However, contrary to [8, 10], we directly work on the measurements instead of a dirty image generated from these data, i.e., there is no gridding step in our algorithm (the objective is to study the robustness of our algorithm to off-grid source reconstruction, which is also natural since we do not know the hidden true sky). Secondly, we apply an adaptive tolerance parameter based on the noise level such that a fast convergence is achieved. Thirdly, we introduce a stopping criterion based on the cumulative sum of the solution energy, which selects the desired level of detail in the image. We evaluate our new algorithm with simulated data for a uniform linear array (ULA) and real data from a LOFAR station, and demonstrate its advantages: accuracy, robustness to extremely low SNR (-20 dB), and fast convergence.

Notation: $\mathscr{E}\{\cdot\}$ denotes the expectation operator, $\langle\cdot,\cdot\rangle$ denotes the inner product, $diag(\cdot)$ converts a vector to a diagonal matrix, $\odot$ denotes the Khatri-Rao product, $\otimes$ denotes the Kronecker product, $\overline{[\cdot]}$ denotes conjugation, and $[\cdot]^H$ denotes complex conjugate transpose.

This work is funded by IBM, ASTRON, the Dutch Ministry of Economic Affairs and the Province of Drenthe.

2. DATA MODEL AND PROBLEM STATEMENT

We consider a radio interferometer consisting of P antennas and model the sky as a collection of Q point sources. We assume that the sources are narrow-band, far-field and independent. Let the wavelength be λ_c. The received signal for antenna p located at $\boldsymbol{r}_p = (r_{x,p}, r_{y,p}, r_{z,p})$ can be represented as $x_p(t) = \sum_{q=1}^{Q} a_{p,q} s_q(t) + z_p(t)$, where $s_q(t)$ denotes the source from direction $\boldsymbol{l}_q = (l_q, m_q, n_q)$, $a_{p,q} = e^{-j\frac{2\pi}{\lambda_c}\langle \boldsymbol{r}_p, \boldsymbol{l}_q \rangle}$ is the steering response for antenna p to source q, and $z_p(t)$ is the additive zero-mean Gaussian noise. Let $\boldsymbol{a}_p = [a_{p,1}, a_{p,2}, \cdots, a_{p,Q}]^T$, $\boldsymbol{x} = [x_1, x_2, \cdots, x_P]^T$, $\mathbf{A} = [\boldsymbol{a}_1, \boldsymbol{a}_2, \cdots, \boldsymbol{a}_P]^T$, $\boldsymbol{s} = [s_1, s_2, \cdots, s_Q]^T$ and $\boldsymbol{z} = [z_1, z_2, \cdots, z_P]^T$. We have our data model $\boldsymbol{x} = \boldsymbol{A}\boldsymbol{s} + \boldsymbol{z}$. Stacking all N time samples into a matrix $\boldsymbol{X} = \big[\boldsymbol{x}[1], \boldsymbol{x}[2], \cdots, \boldsymbol{x}[N]\big]$, we have the sample covariance matrix

$$\hat{\boldsymbol{R}} = \frac{1}{N} \boldsymbol{X} \boldsymbol{X}^H.$$

Since we assume that the sources and noise are uncorrelated, the expected value of the sample covariance matrix is

$$\boldsymbol{R} = \boldsymbol{A} \boldsymbol{\Sigma}_s \boldsymbol{A}^H + \boldsymbol{\Sigma}_n, \tag{1}$$

where $\boldsymbol{\Sigma}_s = \mathscr{E}\{\boldsymbol{s}\boldsymbol{s}^H\} = diag\{\boldsymbol{\sigma}_s\}$ with source intensity $\boldsymbol{\sigma}_s = [\sigma_1, \sigma_2, \cdots, \sigma_Q]^T$ and each $\sigma_q = \mathscr{E}\{|s_q|^2\}$, $\boldsymbol{\Sigma}_n = \mathscr{E}\{\boldsymbol{z}\boldsymbol{z}^H\} = diag\{\boldsymbol{\sigma}_n\}$ with noise intensity $\boldsymbol{\sigma}_n = [\sigma_{z,1}, \sigma_{z,2}, \cdots, \sigma_{z,P}]^T$ and each $\sigma_{z,p} = \mathscr{E}\{|z_p|^2\}$. Each matrix element $\boldsymbol{R}_{i,j}$ represents an interferometric correlation along the baseline vector between antenna i and j in the array.

Vectorizing both sides of equation (1), we get

$$\boldsymbol{y} = (\overline{\boldsymbol{A}} \circ \boldsymbol{A}) \boldsymbol{\sigma}_s + (\overline{\boldsymbol{I}_P} \circ \boldsymbol{I}_P) \boldsymbol{\sigma}_n, \tag{2}$$

where $\boldsymbol{y} = vec(\boldsymbol{R})$ and $\boldsymbol{I}_P$ is a $P \times P$ identity matrix. Let $\boldsymbol{M}_s = (\overline{\boldsymbol{A}} \circ \boldsymbol{A})$ and $\boldsymbol{M}_n = (\overline{\boldsymbol{I}_P} \circ \boldsymbol{I}_P)$. Let $\boldsymbol{M}_s$ be a wide matrix, i.e., $P^2 < Q$.

Assume the sky image (spatial intensity distribution) is sparse or compressible in some sparsity basis $\boldsymbol{\psi}$ (e.g., a Dirac, Fourier, or wavelet basis), i.e., $(\boldsymbol{\psi}^T \boldsymbol{\sigma}_s)$ has only K non-zero values, such that $K \ll Q$. Our objective is to solve $\{\boldsymbol{\sigma}_s, \boldsymbol{\sigma}_n, K\}$ from (2) by using compressed sensing (CS) techniques, i.e., solving the following optimization problem:

$$\min_{\{\boldsymbol{\sigma}_s, \boldsymbol{\sigma}_n\}} \|\boldsymbol{\psi}^T \boldsymbol{\sigma}_s\|_1, \tag{3}$$
$$\text{subject to } \|\boldsymbol{y} - \boldsymbol{M}_s \boldsymbol{\sigma}_s - \boldsymbol{M}_n \boldsymbol{\sigma}_n\|_2 < \varepsilon \quad \text{and} \quad \boldsymbol{\sigma}_s \geq \boldsymbol{0},$$

where ε is the tolerance parameter based on the noise level. The non-negativity constraint $\boldsymbol{\sigma}_s \geq \boldsymbol{0}$ has a physical meaning: the intensity is always positive. We should be aware that our observational data are from a practical antenna layout that might be not random enough to satisfy the Restricted Isometry Property (RIP), which is a sufficient condition for stable recovery in standard CS-problems. Hence, stable recovery could be a challenge. Finally, we are working on the analysis-based framework.

3. ALGORITHM IMPLEMENTATION

We would like to emphasise that we are directly working on the measurements (covariances or *visibilities* in radio astronomy). This is different from the basic CLEAN algorithm, whose procedures are: estimate a dirty image, detect the brightest source component with corresponding intensity and then extract a portion of it from this dirty image. This is repeated until a stopping criterion is met. The final reconstructed image from CLEAN is the collection of all detected source components convolved with an ideal reconstruction beam plus the residual image.

Our problem (3) is almost the same as the one in [8], except for the extra noise term $\boldsymbol{\sigma}_n$. We therefore deal with the noise first. As the autocorrelation (diagonal) elements in $\hat{\boldsymbol{R}}$ is generally considered as sky noise due to its dominance, we mask them by applying a mask matrix $\boldsymbol{M}_{mask}$ to $\boldsymbol{y} - \boldsymbol{M}_s \boldsymbol{\sigma}_s$, such that our problem becomes [12]

$$\min_{\{\boldsymbol{\sigma}_s\}} \|\boldsymbol{\psi}^T \boldsymbol{\sigma}_s\|_1, \tag{4}$$
$$\text{subject to } \|(\boldsymbol{y} - \boldsymbol{M}_s \boldsymbol{\sigma}_s) \times \boldsymbol{M}_{mask}\|_2 < \varepsilon \quad \text{and} \quad \boldsymbol{\sigma}_s \geq \boldsymbol{0}.$$

We then focus on solving $\boldsymbol{\sigma}_s$ from (4) using the proximal splitting method. After getting a feasible solution $\hat{\boldsymbol{\sigma}}_s$, we estimate the noise intensity from

$$\hat{\boldsymbol{\sigma}}_n = \arg\min_{\boldsymbol{\sigma}_n} \|\boldsymbol{y} - \boldsymbol{M}_s \hat{\boldsymbol{\sigma}}_s - \boldsymbol{M}_n \boldsymbol{\sigma}_n\|_2^2. \tag{5}$$

Algorithm 1 Our algorithm

Input: : $\boldsymbol{y}$, $\boldsymbol{M_s}$, $\boldsymbol{\psi}$, τ, η, γ, T, C_K and N_{iter}
Output: : Reconstructed image $\hat{\boldsymbol{\sigma}}_s$, K

```
Initialize: i = 1, σ_s^[0] = 0, ε_0^[1], ε_*^[1] = 0.95 * ε_0^[1],
while i < N_iter do
    Compute: ε^[i] = η ε_*^[i]
    Compute: σ̂_s0^[i] = △(y, M_s, ψ, σ̂_s^[i−1], η, γ, T, ε^[i])
    Truncate: σ̂_s^[i], K ← σ̂_s0^[i] with C_K
    Compute: ρ = ‖σ̂_s^[i] − σ̂_s^[i−1]‖_2 / ‖σ̂_s^[i−1]‖_2
    if ρ < τ then
        break
    else
        i = i + 1
        Compute: ε_*^[i] = (ε_0^[1] − ε^[∞]) e^{(1−i)/2} + ε^[∞]
Return σ̂_s and K
```

The l_2 norm in problem (4) forces the residual to be small, while the l_1 norm enforces sparsity of the representation. This trade-off can be controlled by a regularization parameter γ for $\gamma > 0$:

$$\min_{\{\boldsymbol{\sigma}_s\}} \tau_{\mathbb{S}}(\boldsymbol{\sigma}_s) + \gamma \|\boldsymbol{\psi}^T \boldsymbol{\sigma}_s\|_1, \quad \text{subject to } \boldsymbol{\sigma}_s \geq \boldsymbol{0}, \tag{6}$$

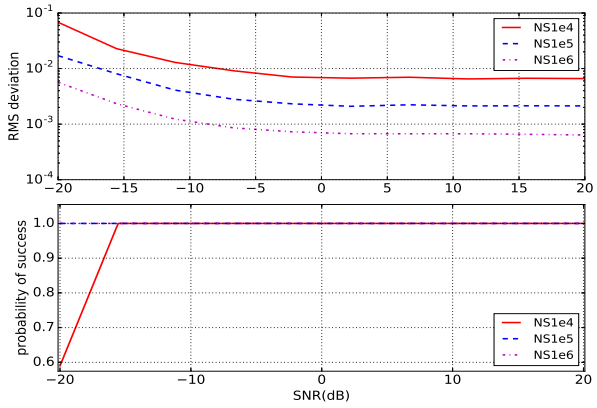

(a) Monte Carlo 100 runs

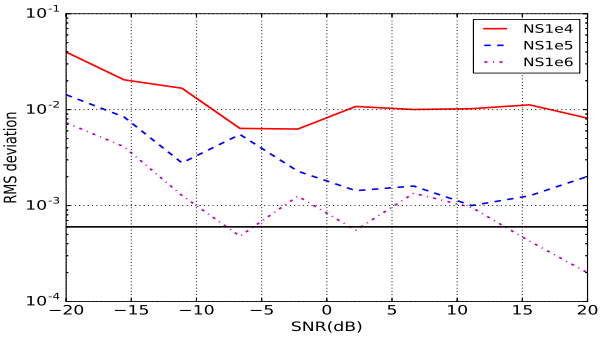

(b) One run

Fig. 1. Monte Carlo simulation results for different SNR values: (a) averaged within 100 runs, where (top) RMS difference between estimated and true value for 10^4, 10^5 and 10^6 samples; (bottom) probability of successful source recovery; (b) one realization.

where $\tau_{\mathbb{S}}(\boldsymbol{\sigma}_s)$ is an indicator function defined in a l_2-ball with $\mathbb{S} \triangleq \{\boldsymbol{\sigma}_s \in \mathbb{R}^{N^2} : \|(\boldsymbol{y} - \boldsymbol{M}_s\boldsymbol{\sigma}_s) \times \boldsymbol{M}_{mask}\|_2 < \varepsilon\}$. We use the Douglas-Rachford splitting algorithm to solve (6). The resulting algorithm is defined in Algorithm 1. The main part $\hat{\boldsymbol{\sigma}}_{s0}^{[i]} = \triangle(\boldsymbol{y}, \boldsymbol{M_s}, \boldsymbol{\psi}, \boldsymbol{\sigma}_s^{[i-1]}, \eta, \gamma, T, \varepsilon^{[i]})$ is solved by the fast iterative shrinkage-thresholding algorithm (FISTA) [13].

Different from [8] which used the noise tolerance $\varepsilon = \sqrt{(2P^2+4P)\sigma_n^2/2}$ where $\sigma_n^2/2$ is the noise variance, in each iteration i, we first calculate [12]

$$\varepsilon_*^{[i]} = (\varepsilon^{[1]} - \varepsilon^{[\infty]})\, e^{(1-i)/2} + \varepsilon^{[\infty]} \quad \texttt{for} \quad i > 1, \qquad (7)$$

where $\varepsilon^{[1]} = \|\boldsymbol{y} \times \boldsymbol{M}_{mask}\|_2$, $\varepsilon^{[\infty]} = \sqrt{\frac{1}{P}\hat{\overline{\boldsymbol{R}}} \otimes \hat{\boldsymbol{R}}}$, then multiply it with η for $\eta \in (0, 1.0]$, i.e., $\varepsilon^{[i]} = \eta\, \varepsilon_*^{[i]}$, such that a fast convergence is achieved. Note η needs to be carefully chosen for different experiments. It is also important to choose γ because it determines the degree of sparsity. Based on our numerical simulation, we found that the bigger γ, the higher sensitivity for strong sources will be achieved. Radio astronomy needs high sensitivity to detect the weak sources, so we fix γ to be the step-size of our algorithm.

Another question is how to characterize the maximum number of sources. It has been well known that underestimating the number of sources will result in a strong deterioration of the quality of spectra, including widening and possible disappearance of some sources, but a large overestimate leads to the appearance of spurious peaks due to noise. In this paper, we propose an adjustable way to determine K by the cumulative sum C_K of the estimated solutions energy if K is unknown. Once we have decided how much detail is needed in our estimated image, we can find K through C_K from this curve. The algorithm stops when the maximum number of iterations N_{iter} is reached or when the relative error of successive solutions $\|\hat{\boldsymbol{\sigma}}_s^{[i]} - \hat{\boldsymbol{\sigma}}_s^{[i-1]}\|_2 / \|\hat{\boldsymbol{\sigma}}_s^{[i-1]}\|_2$ is smaller than some bound τ. We initialize $\boldsymbol{\sigma}_s$ as $\mathbf{0}$ and set step size $T = 0.01$.

4. ALGORITHM EVALUATION

We evaluate our algorithm in terms of source position and intensity recovery with two different antenna array layouts: a uniformly linear array (ULA) and an irregular array - a LOFAR station. We run it on a MacBook Air with a 1.6-GHz Intel Core i5 CPU and 8 GB of 1600 MHz DDR3 RAM.

4.1. Uniform linear array (ULA)

The ULA consists of 20 antennas separated by half a wavelength of the narrow-band source signals observed at a wavelength of $\lambda_c = 2.0$ meters. The antenna locations are $r_{x,p} = -10.5 + p$ for $p = 1, 2, \cdots, 20$. Four uncorrelated sources with intensities $[0.85, 0.12, 0.56, 1.0]$ are lying on the grid positions $(-1.0, 0.0)$, $(-0.4, 0.0)$, $(-0.2, 0.0)$ and $(0.4, 0.0)$, where the line area $[-1.0, 1.0)$ is uniformly split into 40 grid points. Note that the ratio of the weakest source to the strongest is 0.12. Zero mean Gaussian noise is added to each antenna based on the desired SNR, whose value varies in 10 logarithmically spaced steps from -20dB to $+20$dB. Here, the SNR is defined as the power ratio of the average power of the four sources and the average noise power. Hence, our SNR is smaller than the general "peak SNR". The number of samples for one snapshot is 10^4, 10^5 or 10^6. For each SNR value and each number of samples, we did 100 runs in our Monte Carlo simulation. In this experiment, we assume that all sources are lying on grid points. However, through numerical simulation, we found that our algorithm shows very good robustness for off-grid source recovery when the reconstruction grid is coarser than the original grid. If the reconstruction grid is finer than the original grid, some fake source may appear besides the true sources whose intensity is slightly lowered. This effect can be avoided by carefully selecting the thresholding value.

We use the measure

$$\varepsilon_I = \sqrt{\frac{1}{K}\sum_{q=1}^{Q} \|I_q - \hat{I}_q\|_2^2}, \qquad (8)$$

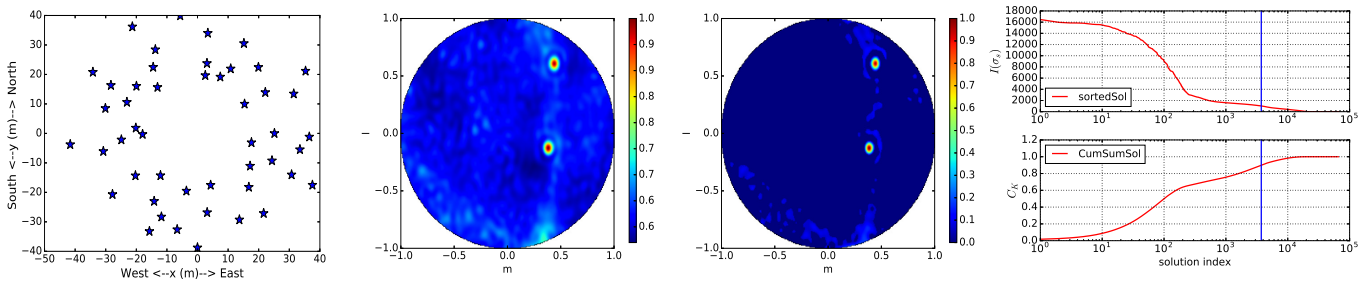

(a) LOFAR layout (b) Dirty image (c) Reconstructed image (d) Estimated solution

Fig. 2. Example of all sky image recovery with a LOFAR station with 48 antnenas at 53.125 MHz: (a) LOFAR station antenna layout (48 antennas), (b) beamforming based dirty image; (c) image reconstructed using our algorithm; and (d) estimated solution and cumulative sum of solutions by our algorithm, where the vertical blue line denotes the truncation thresholding for cumulative sum 0.90.

where K is the true number of sources and Q represents the number of grid points. In the equation above, K instead of Q is used for determining the accuracy, because the lower K is actually augmenting the root-mean-square (RMS) error compared to the standard definition using Q. In the current case, $K = 4$ and $Q = 40$.

If, in our Monte Carlo simulation, only one source position is estimated wrongly in one run out of the 100 runs done for a single SNR, the error for that run would be $\|I_q - \hat{I}_q\| > I_{min} = 0.12$. This is the best case after 100% successful reconstruction. Based on equation (8), the RMS error in the run with error would be about $\sqrt{0.12^2/4}$. When this is averaged over 100 runs that are otherwise successful, this results in an average RMS error of $0.0006 = 10^{-3.22}$. This is the low bound for our algorithm. If the RMS error is lower than this value, the reconstruction can thus be considered "perfect".

The top panel of Fig.1 (a) shows the average RMS error obtained from our Monte Carlo simulation as function of SNR over 100 runs for the respective number of samples; and the bottom panel gives the probability of success in position estimation. This sub-figure clearly demonstrates the accuracy and robustness of our algorithm: 1) the RMS deviation monotonically decreases as SNR increases; 2) the accuracy improves with the number of samples; 3) if the SNR is greater than -15 dB, even for only 10^4 samples, all sources could be exactly reconstructed; 4) the very weak source (intensity 0.12) is exactly recovered. Fig.1 (b) shows the average RMS error obtained from one run/realization as function of SNR, during which the black horizontal line is the "perfect" line. This sub-figure shows us that: 1) the RMS error decreases as the number of samples increases; and 2) while this error is not monotonically decreasing as SNR increases.

4.2. Arbitrary antenna layout: LOFAR station

We evaluate our algorithm on real data from a LOFAR station. This layout consists of 48 antennas, as shown in Fig. 2 (a). The central frequency of our test channel is 53.125 MHz and the bandwidth is 195 kHz. The test data consist of a series of array covariance matrices captured between 21:01:29 UTC and 21:10:00 UTC and integrated by 1 second and calibrated by a sky-model. We tested with both a Dirac basis and Daubechies wavelets in sparse representation, but our present simulation shows no big difference.

For a grid of 256×256 and a threshold value be 0.90, it took about 36.8 seconds for 4 iterations to stop. The reconstructed image using our algorithm and the dirty image formed by delay beamforming are shown in Fig. 2 (b) and (c). We would like to emphasise that: 1) the dirty images are generated where all the autocorrelation (diagonal) elements in covariance matrix are removed; and 2) the antenna array is not projected to the horizontal plane since our estimated source intensity is in the normal direction. Comparing Fig. 2 (c) with (b), it clearly shows that our algorithm reconstructs the main features: 1) two bright sources, 2) the less dominant diffuse emission from the Galactic plane, and 3) the background and side-lobes are clearly reduced. Fig. 2 (d) shows the estimated ordered solution distribution and its cumulative sum of energy, whose decaying curve shows three situations: a few strong sources, hundreds of intermediate sources and ten thousands of weak sources. There are $K = 3744$ sources kept, which is approximately $\frac{3744}{256^2} \times 100\% = 5.71\%$ of the total grid points. As mentioned before, the number of sources could be increased if needed by lowering the thresholding value.

5. CONCLUSION

A new sparse recovery algorithm was proposed and evaluated with simulated data and real data. We have demonstrated its superior performance in terms of robustness and accuracy for sources lying on the image grid. Our algorithm was shown to reconstruct both point sources and extended sources with real data. Our next step is to study recovery of the off-grid sources and the position shift issue as well as the use of a wavelet representation for signal recovery in real data.

6. REFERENCES

[1] M. P. van Haarlem et al., "LOFAR: the low-frequency array," *Astron. Astrophys.*, vol. 556, no. A2, pp. 1–53, August 2013.

[2] P. E. Dewdney, P. J. Hall, R. T. Schilizzi, and T. J. L. W. Lazio, "The Square Kilometre Array," *Proc. IEEE*, vol. 97, no. 8, pp. 1482–1496, Aug. 2009.

[3] J. A. Högbom, "Aperture synthesis with a non-regular distribution of interferometer baselines," *Astron. Astrophys. Suppl.*, vol. 15, pp. 417–426, June 1974.

[4] T. J. Cornwell, "Multiscale CLEAN deconvolution of radio synthesis images," *IEEE J. Sel. Top. Signal Process.*, vol. 2, no. 5, pp. 793–801, Oct. 2008.

[5] Y. Wiaux, L. Jacques, G. Puy, A. Scaife, and P. Vandergheynst, "Compressed sensing imaging techniques for radio interferometry," *Mon. Not. R. Astron. Soc.*, vol. 395, no. 3, pp. 1733–1742, May 2009.

[6] S. Wenger, M. Magnor, Y. Pihlstrom, S. Bhatnagar, and U. Rau, "SparseRI: a compressed sensing framework for aperture synthesis imaging in radio astronomy," *Publications of the Astronomical Society of the Pacific*, vol. 122, no. 897, pp. 1367–1374, November 2010.

[7] F. Li, T. J. Cornwell, and F. de Hoog, "The application of compressive sampling to radio astronomy I: Deconvolution," *Astron. Astrophys.*, vol. 528, no. A31, pp. 10, April 2011.

[8] R. E. Carrilo, J. D. McEwen, and Y. Wiaux, "Sparsity averaging reweighted analsysis (SARA): a novel algorithm for radio-interferometric imaging," *Mon. Not. R. Astron. Soc*, vol. 426, no. 2, pp. 1223–1234, October 2012.

[9] H. Garsden et al., "LOFAR sparse image reconstruction," *Astron. Astrophys.*, vol. 575, no. A90, pp. 18, March 2015.

[10] A. Onose, R. E. Carrillo, A. Repetti, J. D. McEwen, J. P. Thiran, J. C. Pesquet, and Y. Wiaux, "Scalable splitting algorithms for big-data interferometric imaging in the SKA era," *Mon. Not. R. Astron. Soc.*, vol. 462, no. 4, pp. 4314–4335, August 2016.

[11] P. L. Combettes and J. C. Pesquet, "A Douglas-Rachford splitting approach to nonsmooth convex variational signal recovery," *IEEE J. Sel. Top. Signal Process.*, vol. 1, no. 4, pp. 1–12, Dec. 2007.

[12] S. J. Wijnholds and S. Chiarucci, "Blind calibration of phased arrays using sparsity constraints on the signal model," in *Proc. 24th European Signal Process. Conf (EUSIPCO'2016)*, Budapest, Hungary, August 2016, pp. 270–274.

[13] A. Beck and M. Teboulle, "A fast iterative shrinkage-thresholding algorithm for linear inverse problems," *SIAM J. Imag. Sci.*, vol. 2, no. 1, pp. 183–202, March 2009.